



Unstructured large eddy simulation technology for aeroacoustics of complex jet flows

Guillaume A. Brès^{1†}, Yaser Khalighi^{2†}, Frank Ham^{3†} and Sanjiva K. Lele^{4*}

[†]Cascade Technologies Inc.
Palo Alto, CA 94303

^{*}Stanford University, Dept. of Mechanical Engineering
Palo Alto, CA 94305

ABSTRACT

The present paper reviews the unstructured large eddy simulation (LES) technology that has been developed for high-fidelity computations of complex jet flow problems. The LES framework features low-dissipation and low-dispersion numerical discretization on unstructured meshes, localized adaptive refinement to capture fine-scale turbulence, and localized shock-capturing schemes. To demonstrate the capability to efficiently handle realistic nozzle geometries, large eddy simulations are performed for a separate-flow nozzle of bypass ratio 5 with round fan and core nozzle operating at the takeoff cycle point. As an example of complex jet configurations with strong shock/turbulence interactions, LES of supersonic impinging jets are conducted at different nozzle pressure ratios. In both cases, qualitative and quantitative comparisons between simulations and experiments are shown, as well as grid convergence studies. Overall, the flow and noise predictions show good agreement with the available experimental measurements.

Keywords: Aeroacoustics, LES, Jet noise

1. INTRODUCTION

Over the last 40 years, the noise of propulsive jets powering civilian aircraft has been reduced by approximately 20 dB, in large measure by the introduction of the turbofan engine with progressively higher bypass ratio. Yet, more stringent noise regulations, the long term vision of effectively “silent” aircraft, and environmental impact concerns continue to push the civilian (and military) aircraft towards design configurations that further reduce the noise, while maintaining other performance metrics (like nozzle thrust). Until recently, the development of such designs has relied largely on laboratory and full-scale testing. However, cost constraints and the high complexity of the flow often limit the range of the parametric investigation and the success of the design optimization. Flow and noise-prediction tools which are fundamentally rooted in the flow-physics are needed to help improve the understanding of the sources of jet noise and guide the analysis processes towards significantly quieter designs.

In this context, large eddy simulation (LES), along with advancement in high-performance computing, is emerging as an accurate yet cost-effective computational tool for prediction of turbulent flows and their acoustic field. As reviewed by Bodony and Lele [1], accurate prediction of jet noise requires particular attention to details in many different aspects (e.g., inclusion of nozzle geometry, low numerical dissipation, appropriate boundary condition treatment [2] and shock capturing schemes [3], etc.).

Based on the experience gained in the mentioned research, and to expand LES for practical industrial applications (including complex jet configurations), an unstructured large eddy simulation technology has been developed [4, 5, 6]. The paper presents a review of the technology and its application to two representative jet flow problems. The LES framework is discussed in section 2. To demonstrate the capability to handle complex nozzle geometries, large eddy simulations of a dual stream nozzle are performed and compared to experiments carried out at NASA Langley Jet Noise Laboratory [7] in section 3. Finally, flow and noise predictions of supersonic impinging jets, representative of complex jet configurations, are compared to experiments conducted at the Florida State University [8, 9] in section 4.

¹ gbres@cascadetechnologies.com

² khalighi@cascadetechnologies.com

³ fham@stanford.edu

⁴ lele@stanford.edu

2. UNSTRUCTURED LES TECHNOLOGY

The unstructured LES technology used here is composed of pre-processing tools (i.e. mesh generation), a compressible flow solver “Charles”, and post-processing tools. The mesh generation modules features localized adaptive refinement capabilities and produces high-quality yet economical unstructured grids suitable for capturing turbulence dynamics. The flow solver utilizes a low-dissipative numerical scheme designed to produce accurate results on unstructured meshes, in particular in the presence of hanging nodes and other transition type elements. The large database generated by LES is then processed by the post-processing module for statistical analysis of flow and noise, as well as flow visualization.

2.1 Compressible flow solver

The compressible flow solver “Charles” solves the spatially-filtered compressible Navier–Stokes equations on unstructured grids using a novel control-volume based finite volume method where the flux is computed at each control volume face using a blend of a non-dissipative central flux and a dissipative upwind flux, i.e.:

$$F = (1 - \alpha)F_{central} + \alpha F_{upwind}, \quad (1)$$

where $0 \leq \alpha \leq 1$ is a blending parameter. This blending approach is often the basis of implicit approaches to LES, where the blending parameter is selected as a global constant with a value large enough to provide all the necessary dissipation (and potentially much more).

Here, Charles does not use the implicit LES approach, but a novel algorithm [4] to compute a locally optimal (i.e. minimal) α . To minimize numerical dissipation relative to implicit LES approaches, the value of α is allowed to vary spatially such that it can be set to zero in regions where the grid quality is good and the scheme based on the central flux is discretely stable and non-dissipative. In regions of less-than-perfect grid quality, however, the central scheme can introduce numerical instabilities that must be prevented from contaminating/destabilizing the solution by locally increasing α . One significant advantage of this approach is that the blending parameter is purely grid-based, and can be pre-computed based on the operators only.

2.2 Sub-grid scale modeling and shock-capturing schemes

Because the underlying numerical method has minimal numerical dissipation, it is critical to employ a sub-grid model to account for the physical effects of the unresolved turbulence on the resolved flow. Two modeling options are available in the code: the dynamic Smagorinsky model [10, 11, 12] and a dynamic version of Vreman’s model [13, 14]. For the large eddy simulations reported in this work, the Vreman model is used with constant coefficient set to the recommended value of $c = 0.07$, and constant turbulent Prandtl number $Pr_t = 0.9$ to close the energy equation.

Shocks, like sub-grid scale turbulence, are also sub-grid phenomena and thus require modeling to account for their effect on the resolved flow. However, unlike sub-grid scale turbulence, they are localized in the flow and a surgical introduction of modeling is potentially more appropriate. Charles uses a hybrid Central-WENO scheme to simulate flows involving shocks. The scheme has three pieces: a central scheme (described previously), a shock-appropriate scheme and a hybrid switch. For the scheme appropriate for computing a flux across a shock, Charles uses a fully unstructured 2nd-order ENO method to perform reconstructions. The hybrid switch, which detects where shocks are present in the flow and activates the shock-appropriate scheme, is based on the method developed originally by Hill and Pullin [15].

2.3 Calculation of far field noise

Surface projection techniques are widely used for calculation of far field noise, since accurate direct computation of sound at far field locations would be prohibitively expensive. For prediction of jet noise, an acoustic projection module [4] was developed based on the early work of Ffowcs Williams and Hawkins (FW-H) [16] and its extension for hot supersonic jet by Spalart and Shur [17]. In the original FW-H permeable formulation, sound at far field locations is computed from flow information on an arbitrarily-shaped surface (S) and the volume-distributed sources outside of S . Due to the difficulties associated with using volume-distributed sources, surface S is often chosen such that it encloses flow-generating sound sources. As a result, the volume term can be assumed small enough and its effect can be neglected.

For simulation of hot jets, Spalart and Shur [17] argue that neglecting the volume term can be erroneous, where surface S fails to entirely enclose the region of turbulence. They demonstrate that a pressure-based variant of the original permeable formulation can reduce this error. Based on this study and recent work by

Mendez *et al.* [18], the pressure-based formulation seems best-suited for noise prediction of hot supersonic jets and is applied in the present work.

Time accurate flow variables are collected on a surface S that encloses the sources of sound (see figure 1). The data is retrieved using a method of snapshots from the stored transient volumetric flow-field. The far field noise is then computed directly in the frequency domain using the FW-H solver, with the volume term neglected.

3. DUAL-STREAM JET

To demonstrate the capabilities of the LES framework for complex realistic nozzle, large eddy simulations are performed for a separate-flow nozzle of bypass ratio 5 with round fan and core nozzle operating at the takeoff cycle point. The simulation results are compared to experiments carried out in the Low Speed Aeroacoustics Wind Tunnel at NASA Langley Jet Noise Laboratory. This work is a first step towards prediction of flow and noise from closely coupled propulsion-airframe systems.

3.1 Simulation setup

The computational domain includes the jet-plume and a part of the nozzle, as shown in figure 1. The boundary conditions for the LES domain are extracted from a RANS simulation using the tuned coefficients for hot jet proposed by Tam and Ganesan [19], which was carried out in a larger computational domain. A constant plug-flow is applied to the inlet of the nozzle such that the desired pressure ratios and temperatures are achieved at the nozzle lip. The flow issued from the nozzle is assumed to be laminar. Consequently, the grid resolution inside the nozzle is only adequate for a laminar flow. To damp turbulent structures and sound waves approaching the outlet boundary, a sponge layer is applied at the outlet of computational domain by switching the numerical operators to low-order dissipative discretization.

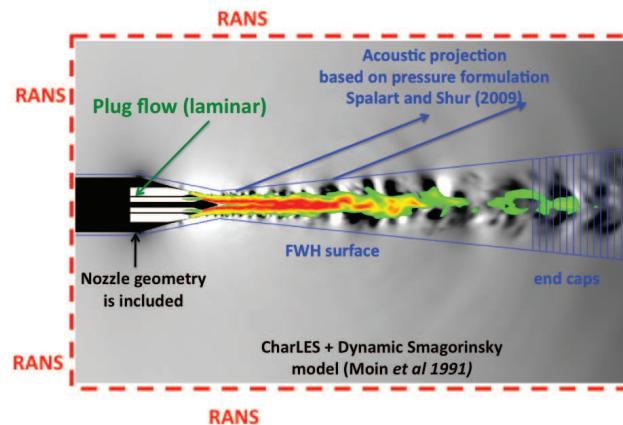


Figure 1: LES computational domain. Axial velocity field is shown in color, and pressure in grayscale.

The coflow applied to the jet surroundings to simulate the wind tunnel Mach number is $M_t = 0.28$. The other simulation parameters match the experimental operating conditions, namely the nozzle pressure ratio $NPR = 1.56$ (1.75), and temperature $T_0 = 828\text{K}$ (350K) for core (fan) flows.

The acoustic projection surface described in section 2.3 is also shown in figure 1. To avoid the spurious noise caused by passage of flow structures through the end cap, the method introduced by Shur *et al.* [20] is applied.

Two different grids are used for this work: a relatively coarse mesh consists of approximately 9 million grid cells and refined mesh with approximately 25 million grid cells. Both meshes are locally refined as shown in Figure 2. In this figure, the coarse mesh is presented and the numbers “16”, “32”, “64”, etc., correspond to the number of points in the azimuthal direction. The fine mesh has the same azimuthal resolution, but is refined in the axial and radial directions by almost a factor of two in the core of the jet plume. The time step for the coarse and fine simulations are $\Delta t c_\infty / D_c = 1.5 \times 10^{-4}$ and $\Delta t c_\infty / D_c = 1.25 \times 10^{-4}$ respectively, where D_c is the core nozzle diameter and c_∞ is the free-stream speed of sound. The statistics for averaging and sound calculation are collected for a period $T c_\infty / D_c = 38.46$ and $T c_\infty / D_c = 26.85$.

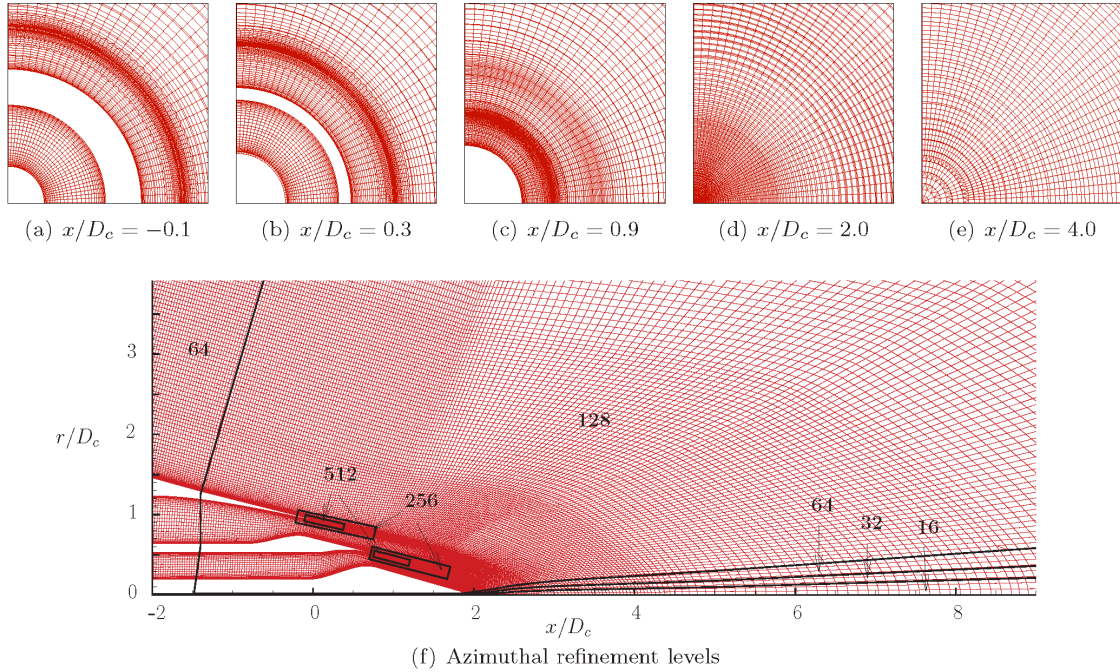


Figure 2: Grid with zonal refinement generated for jet simulations.

3.2 Flow field results

Flow snapshots from the coarse and fine simulations are shown in figure 3. In these snapshots, axial velocity is shown in color to visualize the turbulence in the jet plume and pressure is shown in grayscale to visualize the acoustic field. Only part of the computational domain near the nozzle is presented.

From this figure, it is clear that the coarse calculation does not exhibit the wide range of scales and rich energy content observed in the refined calculation, and is therefore under resolved. Nevertheless, in both cases, inspection of the full computational domain shows that sound waves radiate dominantly downstream, to the high inlet angles, and are originated from the closure region of the potential core.

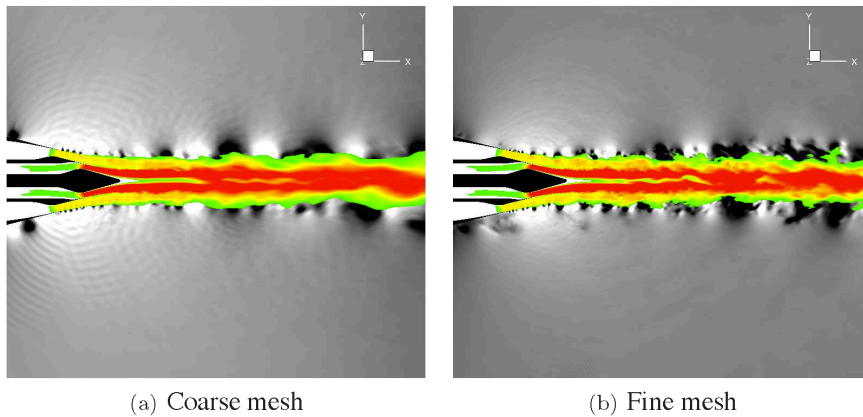


Figure 3: Flow snapshots from coarse and fine LES computations. Axial velocity field is shown in color, and pressure in grayscale.

Here, it is also important to note that the shear layer issued from both fan and core nozzle lips are initially laminar. This situation may not match the experimental conditions and the flow separates from

the core of the nozzle. An early separation and vortex shedding is also visible in the outer wall of the nozzle which is again due to the assumption of laminar flow. Eventually, the shear layers become turbulent and emit a spurious high frequency sound for both fine and coarse calculations. Since this transition is numerical, the emitted sound is also grid-dependent; clearly, the frequency of this high-frequency tone is higher for the fine calculation.

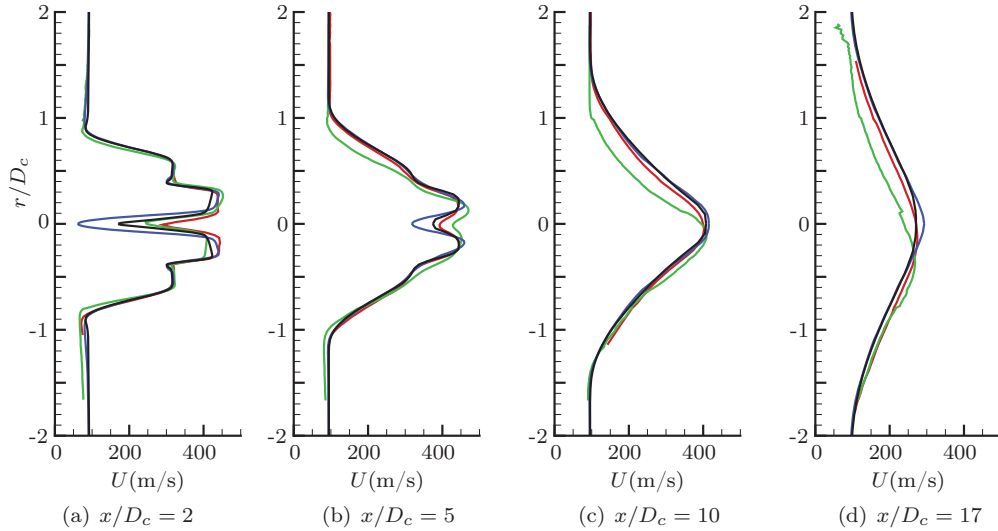


Figure 4: Mean axial velocity: experimental PIV (— green —) and rake (— red —); fine LES (— blue —); RANS with $k - \epsilon$ modified by Tam and Ganesan [19] (— black —).

The radial profile of mean axial velocity at 4 different stations downstream of the nozzle for the fine calculations is plotted in figure 4. The results are compared to PIV and rake measurement reported by Doty *et al.* [7] as well as RANS predictions. The results show good agreement between LES, RANS, and experiment (in particular rake measurements) at stations $x/D_c = 5, 10,$ and 17 . At $x/D_c = 2$, the LES exhibits much lower axial velocities at the center-line; this under-prediction can be explained by the presence of laminar and thicker boundary layer at the core of this flow. The thicker boundary layer results in less momentum in the core flow in particular in the vicinity of the center-line. This is not the case for RANS results as the flow is assumed to be entirely turbulent.

3.3 Far field noise predictions

In figure 5, the far field sound predicted using both fine and coarse meshes are compared to experimental measurements. The noise signal is computed at $r/D_c=100$ from the nozzle exit and is presented in $1/3$ octave bins. Note that because of the shorter run time in the fine simulation, the sound spectra at low frequencies might not be fully converged in that case.

As discussed in the previous section, the footstep of tonal frequency associated with the (unphysical) laminar-turbulent transition at the shear layers issued from the nozzle lips is visible, around 10^4 Hz and $2.5 \cdot 10^4$ Hz. The effect of the tonal noise is more noticeable for the fine calculations due to higher amount of energy produced in the nozzle lip region.

Aside from the differences in the tonal noise and the earlier frequency cutoff for the coarse mesh, both simulations show similar results, in good agreement with experiments, in particular at higher inlet angles (i.e., $\theta = 124.02^\circ$). At lower inlet angles (i.e., $\theta = 51.54^\circ$), more discrepancies are observed. In general, jet noise at higher inlet angles is initiated from the nozzle lip. In contrast, at lower inlet angles, sound waves are mainly due to turbulent action further downstream in the jet plume. Therefore, the trend observed in the numerical predictions is likely due to the higher mesh resolution close to the nozzle lips than close to the potential core closure. A more resolved calculation consisting of 200 millions cells is underway, with tripped boundary layers in the nozzles to resolve the laminar inflow issue.

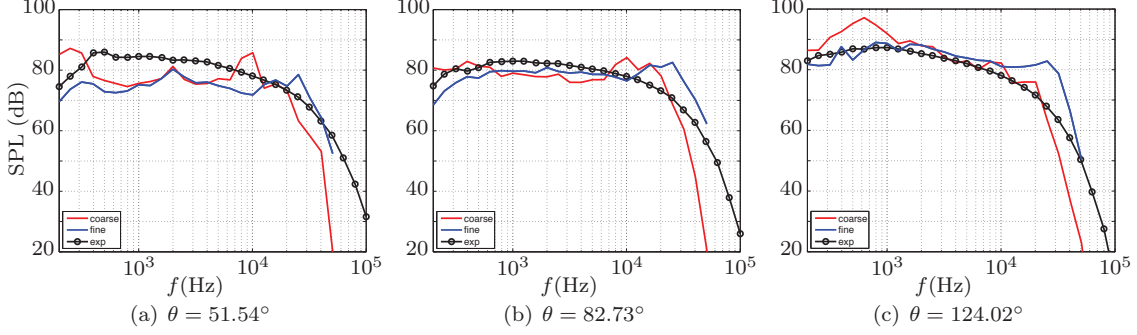


Figure 5: Sound spectra at far field microphones located at $r/D_c = 100$: LES with coarse resolution (—) and fine resolution (—); Experiment (—●—).

4. SUPERSONIC IMPINGING JET

To demonstrate the capability to handle complex jet configurations with strong shock/turbulence interactions, LES of realistic high-speed impinging jets are performed. These configurations are relevant to combat aircrafts designed for short takeoff and vertical landing (STOVL). Such aircrafts achieve the short takeoff by redirecting the propulsive nozzles downwards towards the ground to create a substantial lift force. The interaction of the hot supersonic jet plume with the ground also introduces additional complexities in the flow field (shock-cells, wall-jet, stand-off shock, etc.) and generates additional intense noise often containing multiple tonal components. The noise generated by the plume/ground interaction radiates in all directions and impinges strongly on the propulsive nozzles and the airframe.

4.1 Experimental and numerical setup

Krothapalli *et al.* [8] and Gustavsson *et al.* [9] examined the characteristics of a flow and noise issued from various nozzles and impinging on a ground plane at the STOVL supersonic facility of the Florida State University. For the present case, the experimental axisymmetric nozzle has a throat diameter $d_t = 2.54$ cm designed for an exit Mach number of 1.5 in perfectly-expanded conditions. The diverging part of the nozzle is a 3° angle conical shape that mimics realistic nozzle geometry used in practice. The nozzle exit diameter is $d = 2.75$ cm. The nozzle is connected to a circular lifting plate with diameter D , which is parallel to a large impingement plate at a distance h . In this case, $D/d \approx 10$ and $h/d_t = 4$.

The same experimental setup is used in the simulations. The nozzle pressure ratio NPR is varied from 2.0 to 10.0, and the stagnation temperature ratio of $T_r = 1.0$ is applied to all the cases. The simulations are carried out on a moderate-size mesh of maximum grid size of $\Delta_{max}/d = 0.05$. The minimum resolution is applied radially within the shear layer $\Delta_r^{min}/d = 0.004$. The mesh density is then increased in the vicinity of shear layers and also in the impingement region. The size of this mesh is 7.7 million cells and the time step is $\Delta t c_\infty/D = 5 \times 10^{-4}$. A fine simulation is also performed to study the resolution effect for $NPR = 3.67$ (i.e., perfectly-expanded conditions). In the fine calculation, the mesh was homothetically refined, and the number of cells increases to 57 million, with a time step $\Delta t c_\infty/d = 2.5 \times 10^{-4}$.

4.2 Qualitative description of impinging jet flow

Instantaneous temperature and pressure contours for different nozzle pressure ratios are presented in figure 6. For the perfectly expanded case at $NPR = 3.67$ shown in figure 6(a), the flow issued from the nozzle is initially laminar; the shear layers go through a transition and at distance of approximately two diameters from the nozzle exit, the jet flow is entirely turbulent. Weak shocks form in the jet plume due to the fact that the divergent part of the nozzle is a straight cone. In the vicinity of the impinging plate, a strong stand-off shock is formed that slowly undulates in the vertical direction and the stagnation bubble formed at the impingement “breathes” and interacts with the turbulent shear layer issued from the nozzle. The turbulent structures that pass through the shock are compressed and heated. Due to its local nature, the shock-capturing scheme introduces minimal dissipation and consequently does not destroy the turbulent structures passing through the shock. The turbulent shear layer impinging the ground spread

radially and manifest itself as wall jets. The pressure contours show that the sound is mainly generated by the impingement of the jet. The sound waves travel through the medium and reflect off the lifting plate and the impinging plate.

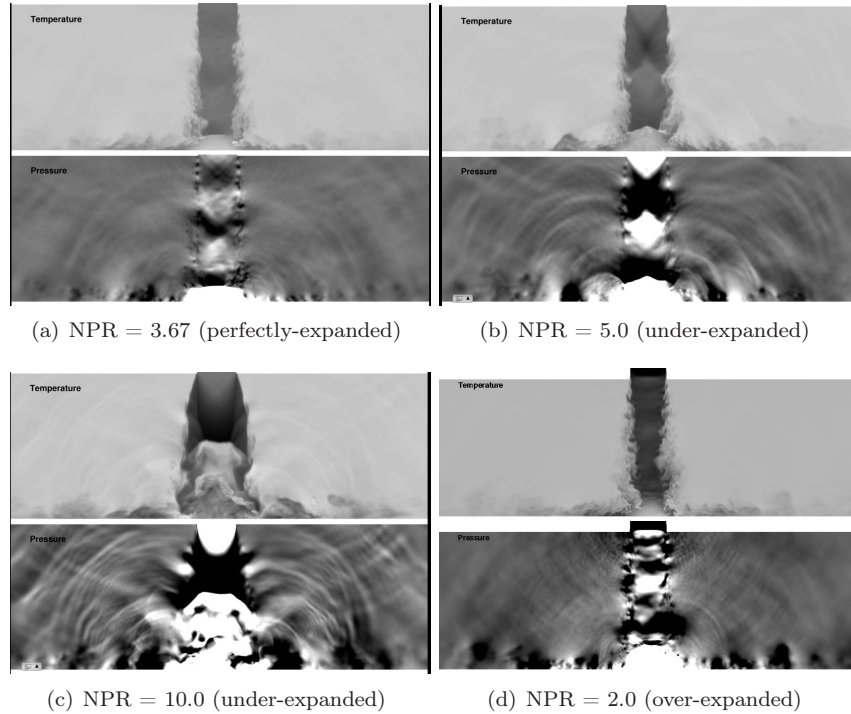


Figure 6: Instantaneous pressure and temperature fields for the impinging jet at various nozzle pressure ratios.

In the under-expanded jet with nozzle pressure ratio of 5.0 shown in figure 6(b), the shock-wave issued from the nozzle is stronger and the stand-off shock does not oscillate as much as in the pressure-matched case. Also, sound emitted from the impingement region is more significant. By increasing the nozzle pressure ratio to 10.0 (i.e., figure 6(c)), a strong shock disk is formed at the nozzle exit. The stand-off shock moves upward and flow within the stagnation bubble appears to recirculate. The sound waves in this case are clearly more energetic than previous configurations.

The over-expanded case in figure 6(d) is representative of more realistic operating conditions and shows lower sound pressure levels than both perfectly-expanded and under-expanded cases. This is because the exit velocity in this case is lower. Here the scales for the temperature and pressure contours are changed compare to the previous three cases, to enable visualization of the structures. Shocks form in the jet plume, however they are weak and almost normal to the jet. A unique feature of the under-expanded jet is the separation of the flow inside the nozzle. Due to adverse pressure gradient and low momentum of the flow inside the boundary layer, flow separates and changes the behavior of the shear layer outside the nozzle. This separation can potentially affect the transition in the shear layer and as a result, affect both near and far field sound.

The temperature field and various cuts normal to the axis for the perfectly expanded nozzle is shown in figure 7. The temperature cuts show that the flow issued from the nozzle exit is initially laminar but in later stages, smaller azimuthal structures appear and eventually the jet plume transitions to turbulence. The axial cuts also show that the instability mode for this configuration is axisymmetric. In last three axial stages (i.e. $x/d = 3, 3.3$ and on the impingement plate) the cuts show the flow field and spread of turbulent structures within the stagnation bubble.

In figure 8, large-scale flow structures computed from LES are qualitatively compared to an experimental flow snapshot obtained from PIV. Here, the stand-off shock, wall jets and the size of unsteady structures in the jet column obtained from LES agree well with the PIV results.

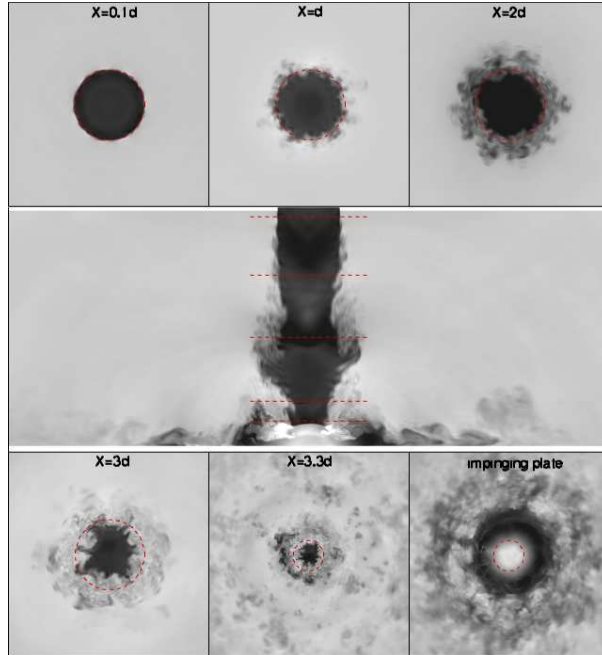


Figure 7: Instantaneous temperature field in various planar cuts normal to the jet axis.

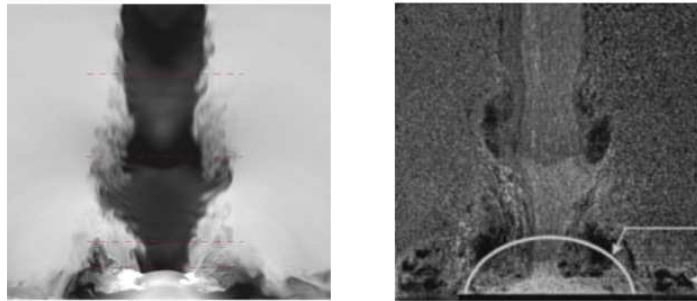


Figure 8: Qualitative comparison of flow structures obtained from LES (left) and PIV (right) [8] .

To assess the quality of the LES and verify that sufficient mesh resolution was used, grid refinement is performed for the pressure-matched case. For this purpose, the grid has been homogeneously refined in all directions. Figure 9 compares the snapshots of flow from coarse and fine simulations. The two simulation were started from the same initial conditions and advanced for the same time period. It is clear from the snapshots that the flow looks very similar in both cases. Comparison of the low-order statistics (mean and rms) from the two simulations also show the same trend. This similarity demonstrates the consistency of the LES results. As expected, the fine grid shows more small structures. This is more evident in the temperature contours.

4.3 Radiated sound predictions

For computation of sound at locations further from the jet, the acoustic projection surface described in section 2.3 is used, along with the method of end caps introduced by Shur *et al.* [20], to avoid errors associated with passing wall jets through the surface.

In the formulation of Ffowcs Williams and Hawkins [16], it is assumed that the sound propagates in an unbounded domain outside of the projection surface. This is not the case in the present problem as sound

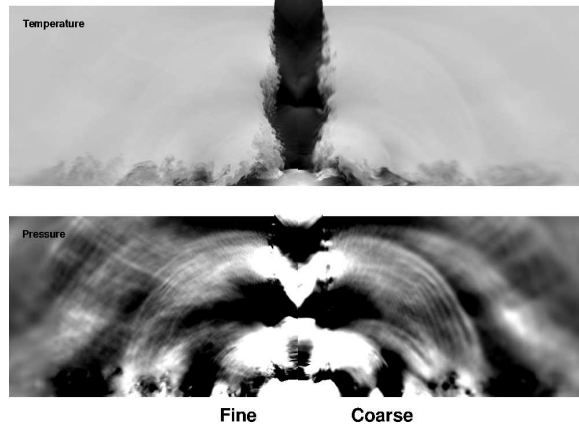


Figure 9: Effect of mesh resolution on instantaneous pressure and temperature field.

waves reflect from the impinging and lifting plates. In this work, an approach based on the method of images is used to account for reflections. First, the control surface encloses not only the jet plume and wall jets, but also the lift plate, such that the reflections from this surface are now considered part of the sound source. Then the noise contribution from the impinging plate is considered with the method of images.

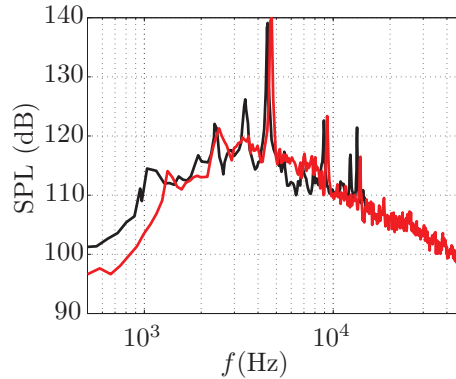


Figure 10: Comparison of radiated sound for perfectly-expanded conditions from LES and FW-H calculation (—) and from experiment of Gustavsson *et al.* [9] (—).

Figure 10 compares the sound pressure level from the perfectly-expanded case with the recent experimental measurements of Gustavsson *et al.* [9] at the same operating condition. The sound is measured at 90° angle and $15 d_t$ away from the nozzle exit. The numerical results are in good agreement with the recent experiment. The shape of the spectra is well predicted and the frequency and the amplitude of the tonal components agree well with the measurements. The numerical results extends to 50 KHz and does not show any sudden drop due to excessive numerical dissipation.

5. CONCLUSIONS

The paper presents a review of the unstructured large eddy simulation (LES) technology that has been developed for high-fidelity computations of complex jet flow problems. The LES framework features low-dissipation and low-dispersion numerical discretization on unstructured meshes, localized adaptive refinement to capture fine-scale turbulence, and localized shock-capturing schemes.

To demonstrate the capability to handle complex nozzle geometries, LES are performed for a separate-flow nozzle and compared to experiments. Overall, promising results are obtained for this realistic nozzle, in terms of predicted flow field and radiated noise. However, the assumed laminar flow issued from the nozzle caused an unphysical transitions to turbulence and an associated tonal frequency, as well as early

detachment of the flow from the center-body. A more resolved calculation with tripped boundary layers is underway to resolve these issues.

As an example of complex jet configurations with strong shock/turbulence interactions, large eddy simulations of impinging jets are conducted at different nozzle pressure ratios including over-, perfectly-, and under-expanded jets. Both flow and sound predictions agreed well with the available experimental measurements. Here, the LES results can potentially provide insight into improved designs to reduce noise, lift-loss, and structural fatigue introduced by impinging high-speed jets. This effort is also particularly relevant for hot supersonic jet impinging on a jet-blast deflector in military applications.

ACKNOWLEDGEMENTS

The authors would like to thank Michael Doty for providing the experimental data for the dual-stream nozzle. This work is supported by NASA SBIR program under grant number NNX10CE73P and NAVAIR SBIR program under grant number N68335-10-C-0563. The majority of calculations were carried out on a CRAY XE6 machine at DoD supercomputer facilities in ERDC.

REFERENCES

- [1] D. J. Bodony, S. K. Lele, "Current status of jet noise predictions using large-eddy simulation," *AIAA J.* 46 (2008) 346–380.
- [2] D. Bodony, "Analysis of sponge zones for computational fluid mechanics," *Journal of Computational Physics* 212 (2005) 681–702.
- [3] A. Mani, J. Larsson, P. Moin, "Suitability of artificial bulk viscosity for large-eddy simulation of turbulent flows with shocks," *Journal of Computational Physics* 228 (2009) 7368–7374.
- [4] Y. Khalighi, F. Ham, P. Moin, S. K. Lele, T. Colonius, R. H. Schlinker, R. A. Reba, J. Simonich, "Unstructured large eddy simulation technology for prediction and control of jet noise," *GT2010-22306* (2010).
- [5] Y. Khalighi, J. Nichols, F. Ham, S. Lele, P. Moin, "Unstructured large eddy simulation for prediction of noise issued from various nozzles," *AIAA paper 2011-xxxx* (2011).
- [6] Y. Khalighi, F. Ham, P. Moin, S. K. Lele, R. H. Schlinker, R. A. Reba, J. Simonich, "Noise prediction of pressure-mismatched jets using unstructured large eddy simulation," *GT2011-46548* (2011).
- [7] M. J. Doty, B. S. Henderson, K. W. Kinzie, "Turbulence measurements of separate-flow nozzles with pylon interaction using particle image velocimetry," *AIAA J.* 45 (2007) 1281–1289.
- [8] A. Krothapalli, E. Rajkuperan, F. Alvi, L. Lourenco, "Flow field and noise characteristics of a supersonic impinging jet," *Journal of Fluid Mechanics* 392 (1999) 155–181.
- [9] J. P. R. Gustavsson, P. A. Ragaller, R. Kumar, F. S. Alvi, "Temperature effect on acoustics of supersonic impinging jet," *AIAA paper 2010-3785* (2010).
- [10] M. Germano, U. Piomelli, P. Moin, W. Cabot, "A dynamic subgrid-scale eddy viscosity model," *Phys. of Fluids* 3 (7) (1991) 1760–1765.
- [11] D. K. Lilly, "A proposed modification of the Germano subgrid-scale closure method," *Phys. Fluids A* 4 (3) (1992) 633–35.
- [12] P. Moin, K. Squires, W. Cabot, S. Lee, "A dynamic subgrid-scale model for compressible turbulence and scalar transport," *Phys. Fluids A* 3-11 (1991) 2746–57.
- [13] A. Vreman, "An eddy-viscosity subgrid-scale model for turbulent shear flow: Algebraic theory and applications," *Physics of Fluids* 16 (2004) 3570.
- [14] D. You, P. Moin, "A dynamic global-coefficient subgrid-scale eddy-viscosity model for large-eddy simulation in complex geometries," *Physics of Fluids* 19 (6) (2007) 065110.
- [15] D. J. Hill, D. I. Pullin, "Hybrid tuned center-difference-weno method for large eddy simulations in the presence of strong shocks," *Journal of Computational Physics* 194 (2) (2004) 435–450.
- [16] J. E. Ffowcs Williams, D. L. Hawkings, "Sound Generation by Turbulence and Surfaces in Arbitrary Motion," *Royal Society of London Philosophical Transactions Series A* 264 (1969) 321–342.
- [17] P. R. Spalart, M. L. Shur, "Variants of Ffowcs Williams-Hawkings equation and their coupling for simulation of hot jets," *International Journal of Aeroacoustics* 4 (3-4) (2009) 247–266.
- [18] S. Mendez, M. Shoeybi, A. Sharma, F. E. Ham, S. K. Lele, P. Moin, "Large-eddy simulations of perfectly-expanded supersonic jets: Quality assessment and validation," *AIAA paper 2010-271* (2010).
- [20] C. K. W. Tam, A. Ganesan, "Modified k-epsilon turbulence model for calculating hot jet mean flows and noise," *AIAA J.* 43 (2004) 26–34.
- [21] M. L. Shur, P. R. Spalart, M. K. Strelets, "Noise prediction for increasingly complex jets. part 1: Methods and tests," *International Journal of Aeroacoustics* 4 (3-4) (2005) 213–246.